Energy & Environmental Science

Cite this: *Energy Environ. Sci.*, 2011, **4**, 5013

www.rsc.org/ees

PAPER

Scalable approach to multi-dimensional bulk Si anodes *via* metal-assisted chemical etching†

Byoung Man Bang, Hyunjung Kim, Hyun-Kon Song, Jaephil Cho* and Soojin Park*

Received 8th August 2011, Accepted 16th September 2011
DOI: 10.1039/c1ee02310a

Specific design and optimization of the configuration of micro-scale materials can effectively enhance battery performance, including volumetric density. Herein, we employed commercially available low-cost bulk silicon powder to produce multi-dimensional silicon composed of porous nanowires and micro-sized cores, which can be used as anode materials in lithium-ion batteries, by combining a metal deposition and metal-assisted chemical etching process. Nanoporous silicon nanowires of 5–8 μm in length and with a pore size of ~10 nm are formed in the bulk silicon particle. The silicon electrodes having multi-dimensional structures accommodate large volume changes of silicon during lithium insertion and extraction. These materials show a high reversible charge capacity of ~2400 mAh g^{-1} with an initial coulombic efficiency of 91% and stable cycle performance. The synthetic route described herein is simple, low-cost, and mass producible (high yield of 40–50% in tens of gram scale), and thus, provides an effective method for producing high-performance anode materials.

1. Introduction

The rapidly expanding markets for mobile electronics, electric vehicles, power tools, and wireless communication devices offer tremendous appeal and opportunity for researchers involved in the development of high performance lithium-ion batteries (LIBs). Carbon-based anode materials are the most widely used in commercial LIBs with limited gravimetric capacity.[1] Therefore, silicon (Si), germanium (Ge), tin (Sn), and their alloys have been significantly investigated as anode materials for LIBs.[2–5] Among these materials, Si exhibits the highest gravimetric capacity of ~4200 mAh g^{-1} with the formation of $Li_{4.4}Si$. However, formidable large volume expansion of Si materials occurs during battery operation, resulting in the pulverization of the electrode materials and desquamation of active materials from the current collector upon prolonged cycling.[6,7] The morphology, conductivity, and surface characteristics of electrode materials play a key role in producing high performance active materials in LIBs.

Switching from bulk materials to nanostructured electrodes including zero-dimensional (0D), 1D, 2D, and 3D structures will revolutionize the LIB industry.[8–11] Since the nanostructured materials have a small size and large surface area, a short diffusion length of lithium ions, and a large contact area between the electrodes and the electrolyte, the large alleviation of lattice

Interdisciplinary School of Green Energy, Ulsan National Institute of Science and Technology, Ulsan, Korea 689-798. E-mail: jpcho@unist.ac.kr; spark@unist.ac.kr; Fax: +82-52-217-2909

† Electronic supplementary information (ESI) available: SEM images of etched bulk Si particles prepared at various etching conditions, and their characterization. See DOI: 10.1039/c1ee02310a

Broader context

Switching from bulk materials to nanostructured electrodes will revolutionize the LIB industry. Since the nanomaterials have a large surface area and a short diffusion length of lithium ions, the nanostructuring of electrodes results in superior performance LIBs, which have higher storage capacity and excellent cycling performance. In contrast, the large surface area of the nanomaterials may result in undesirable side reactions with the electrolyte, leading to the significant fading of capacity and cycling performance. Moreover, these materials suffer from low thermodynamic stability and high cost problems. To solve these problems, the design of electrodes with unique configurations is required. Especially, micro- and nanoscale hybrid materials enable us to use the advantages of each component and to make up for the shortcomings. Herein, we used commercially available low-cost bulk Si powder to produce multi-dimensional Si composed of porous nanowires and micro-sized cores by combing a metal deposition and chemical etching process. These materials show a high specific capacity of ~2400 mAh g^{-1} with an initial coulombic efficiency of 91%. The synthetic route is simple, low-cost, and mass producible (tens of grams per batch), and thus, provides an effective method for producing high-performance anode materials.

stress (*e.g.*, Li-containing alloys such as Si, Sn, and Ge) would be expected during the operation of LIBs.[2–5,12–14] The nanostructuring of electrodes has been demonstrated to result in superior performance LIBs, which have higher storage capacity, higher rate capability, and excellent cycling performance. In contrast, the large surface area of nanostructured materials may result in undesirable side reactions with the electrolyte under certain conditions, leading to the significant fading of Li storage capacity and poor cycling performance. In addition, these materials suffer from low thermodynamic stability and high cost problems.[1,9] To circumvent these problems, designing unique configurations of electrodes, like hollow structures,[15] urchin-like structures,[16] nanowires directly attached to the current collector,[2] and the combination of micro- and nanostructures,[17,18] have been widely investigated. In particular, micro- and nanoscale hybrid materials enable us to use the advantages of each component and to make up for the shortcomings. There are still some obstacles, however, such as low-yield, high-cost, and a complicated process. Previously, nanostructured Si materials have been produced using chemical synthesis from high cost Si precursors with low-yield (<10%),[13,19] a solution-growth method with tens-of-milligram production,[20] a magnetio–thermic reduction method,[21] and solid-state synthesis by reaction of silicon tetraiodide with an alkaline earth metal silicide.[22] Also, nonporous or porous Si nanowires by a metal-assisted chemical etching process have been synthesized using polished silicon wafers with several different crystal orientations and resistivities. In general, metal deposition and chemical etching processes on the Si wafers are well-known methods by controlling etching temperature and the concentration of etchant.[23–27] In contrast, metal-assisted chemical etching of bulk Si powders is rarely reported. Recently, mesoporous Si particles with a high surface area were synthesized by using an iron catalyst, but it was not extended to prepare various Si morphologies.[28] Even though Si materials obtained from these approaches have a high-purity and form high-performance electrodes in LIBs, these materials are not suitable for synthesizing and/or handling in large scale applications.

Herein, we employed commercially available low-cost bulk Si powder to produce multi-dimensional Si (mSi) composed of porous nanowires and micro-sized cores, which can be used as anode materials in LIBs, by combining a metal deposition and metal-assisted chemical etching process. Nanoporous Si nanowires of 5–8 μm in length and with a pore size of ~10 nm are formed in the bulk Si particle. The Si electrodes having multi-dimensional structures accommodate large volume changes of Si during lithium insertion and extraction. These materials show a high reversible charge capacity of ~2400 mAh g^{-1} with an initial coulombic efficiency of 91% and stable cycle performance to 70 cycles. The synthetic route described herein is simple, low-cost, and mass producible (high yield of >50% in over tens of gram scale per batch), and thus, provides an effective method for producing high-performance anode materials.

2. Experimental

2.1 Synthesis of multi-dimensional silicon materials

Commercially available Si powder (30 μm, 99.9%) was purchased from Aldrich. For a typical reaction, Si powder was immersed in a solution of 5–20 mM silver nitrate ($AgNO_3$) and 5 M hydrofluoric acid (HF) for a controlled time of 1–5 min to deposit Ag nanoparticles onto the Si surfaces *via* galvanic reactions. Subsequently, excess silver salts were removed by a copious amount of deionized water several times. Immediately after rinsing, the silver deposited Si powder was immersed in an etchant consisting of 5 M HF and 1.5% hydrogen peroxide (H_2O_2) at 50 °C for 1–3 h to produce multi-dimensional Si materials, and Ag was removed in concentrated nitric acid to make the mSi structure. By controlling the size of Ag nanoparticles, concentration of oxidant (H_2O_2), and chemical etching time, the multi-dimensional Si structures composed of nanoporous Si nanowires and microscale Si matrix were obtained.

As the concentration of $AgNO_3$ was increased from 5 to 20 mM in the electroless plating solutions, the size of silver particles was increased from tens of nanometres to hundreds of nanometres (ESI, Fig. S1†). The effect of H_2O_2 concentration on the morphology of etched Si powder was clearly observed in the longer etching time of 3 h. When the H_2O_2 concentrations are varied with 1.0, 1.5, and 2.0% at a fixed HF (5 M) concentration, Si morphologies having shallow nanopits, nanowires with pore sizes of 15–20 nm, and hundreds of nanometre-sized macropores were obtained, respectively (ESI, Fig. S2†). For carbon coating of the etched Si powder, thermal decomposition of acetylene gas was carried out at 900 °C for 30 min in a quartz furnace. The carbon contents were measured using an elemental analyzer (Flash EA 1112, Thermo Electron Corp.) to determine the carbon and oxygen contents from the samples.

2.2 Characterization of mSi and carbon-coated Si materials

The crystal structures of the chemically etched Si powder were measured by a high power X-ray diffractometer (XRD) on a Rigaku D/MAX at 2500 V using Ni-filtered Cu-Kα radiation with a graphite diffracted beam monochromator. FT-IR spectra were recorded using a Varian 670-IR spectrometer. Raman spectra were recorded on a JASCO spectrometer (NRS-3000) to obtain the degree of graphitization of an amorphous carbon phase in the sample. A He–Ne laser operating at $\lambda = 632.8$ nm was used as the excitation source. Dual-beam Focused Ion Beam (Quanta 3D FEG) was operated using Ga-ions to enable high-precision cross-section processing of etched Si and carbon-coated Si samples. The nitrogen adsorption and desorption isotherms were measured with a VELSORP-mini II (BEL Japan, Inc.) at 77 K in the relative pressure range of P/P_0 from 0.05 to 0.3. It was fitted to the Brunauer–Emmett–Teller (BET) equation to determine the BET surface areas.

2.3 Electrochemical properties of Si electrodes

For the electrochemical properties, coin-type half cells (2016 R-type) that were composed of Si powder as the working electrode and lithium metal as the counter-electrode were prepared under a helium-filled glove box. The electrode for the battery test was made of multi-dimensional Si active material (70 wt%), super P carbon black (15 wt%), and poly(acrylic acid)/sodium carboxymethyl cellulose (Aldrich, wt/wt = 50/50) binder (15 wt%). The electrolyte was $LiPF_6$ (1 M) with ethylene carbonate/diethylene carbonate/dimethyl carbonate (Cheil industries, EC/DEC/DMC,

30 : 40 : 30 vol.%). The coil cells were cycled at a rate of 0.1–3 C between 0.02 and 1.2 V.

3 Results and discussion

3.1 Synthesis of multi-dimensional silicon materials

We used bulk Si powder having an average size of 30 μm to obtain mSi structures composed of nanoscale porous Si nanowires and microscale Si matrix *via* a chemical etching process. Bulk Si powder has a broad size distribution of 2–50 μm, while chemically etched Si has a narrow distribution of 10–15 μm in size as seen in Fig. 1.

The working principle of chemical etching is based on a local oxidation of the Si surface by a metal catalyst and H_2O_2, and the subsequent dissolution of silicon oxide in an HF solution. In this galvanic reaction, metal (*e.g.*, Ag, Au, Cu or Pt) particles act as a local cathode and a catalyst to promote the reduction of H_2O_2 and produce free holes at the interface of Ag and Si, while the Si surface serves as an anode.[29,30] On the anode, the Si is dissolved continuously by transferring electrons to the Ag particles at the interface of Ag and Si in order to reduce H_2O_2 to H_2O. At the cathode, Ag particles are oxidized into Ag^+ ions by H_2O_2, and the Ag^+ ions are reduced to Ag by accepting electrons from Si. With this procedure, the Si underneath the Ag particles is continuously etched down to make porous structures. The overall chemical reactions can be described as follows:

$$Si + 2H_2O_2 + 6F^- + 4H^+ \rightarrow [SiF_6]^{2-} + 4H_2O \quad (1)$$

For this reaction, the standard potential is 2.69 V, indicating that the etching process is thermodynamically favorable.[29]

The size of the silver catalyst was determined by deposition time and affects to the surface and internal morphologies of Si powder. In addition, the concentration of H_2O_2 in an etchant is another key factor to control the Si morphology. From eqn (1), the cell potentials (ΔE) can be expressed as the following Nernst equation.[30]

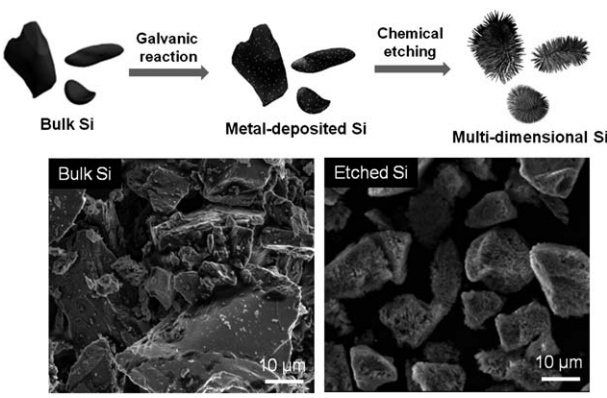

Fig. 1 A schematic of the synthetic route of mSi powder. When the Ag deposited Si powder is immersed in an etchant, Ag catalyzes the Si etching while H_2O_2 used as an oxidant enhances the etching rate to make the mSi structures. Bulk Si powder has a size distribution of 2–50 μm, while etched mSi has much narrower size distribution of 10–15 μm.

$$\Delta E = \Delta E^{o} - \frac{0.059}{4}\left[\log\frac{[SiF_6^{2-}]}{[H_2O_2]} - \log[H^+]^4[F^-]^6\right] \quad (2)$$

where ΔE is the cell potentials and ΔE^{o} is the standard cell potential obtained from the standard reduction potentials.

As the H_2O_2 concentration increases, the cell potential for etching (that is to say, the etching rate) also increases. The combination of 10 mM $AgNO_3$ for silver deposition and an etchant composed of 5 M HF and 1.5% H_2O_2 for etching of Si powder enabled us to make the mSi structures, in which nanoporous Si nanowires are strongly attached to microscale Si matrix with a high-yield of 40–50% on the tens of grams scale (Fig. 2(a)).

In these regards, our method is unique and easily scalable and a cost-saving process. Compared to polished Si wafers, commercially available Si power is >50 times cheaper and a large quantity (30–40 g per batch in laboratory scale) of powder can be used to make mSi powder . Also, various morphologies can be tuned using several different deposition and chemical etching conditions. In particular, when we used Si powder with a purity of 98% (including some impurities, like Fe, Ca, and Al), after chemical etching, every impurity was completely removed by a chemical etchant. It means that low-cost commercially available Si powder can be used to make Si materials with various morphologies.

To investigate morphologies of nanoscale Si nanowires obtained *via* chemical etching, etched samples were dispersed in ethanol followed by ultrasonication for 3 min. The transmission electron microscopic (TEM) image of Si nanowires transferred onto Formvar-coated copper grids showed pores of 15–20 nm (inset of Fig. 2(a)). The cross-section of mSi was obtained from

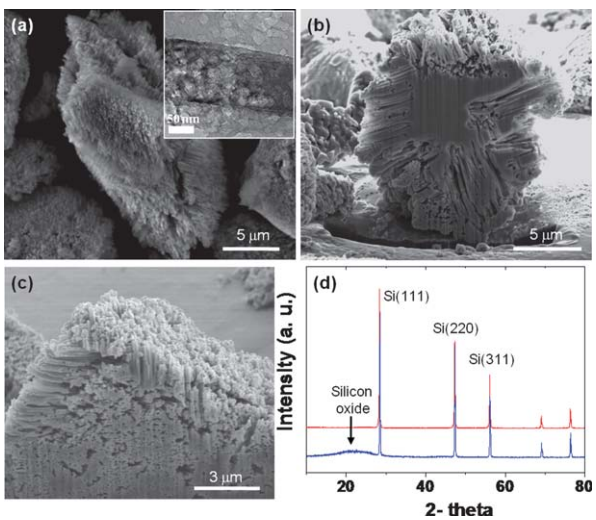

Fig. 2 The morphology of multi-dimensional Si prepared by chemical etching. (a) A SEM image of mSi. The inset shows that Si nanowires have pores of 15–20 nm. (b and c) Cross-sectional SEM images of mSi obtained from the FIB process. Porous Si nanowires and pores are seen over the entire Si, indicating that chemical etching was performed near the center of the Si core. (d) XRD patterns of as-synthesized and HF-etched Si samples. As-prepared Si had a small amount of silicon oxide (bottom in (d)). After immersing Si in HF for 1 min, the silicon oxide was completely removed (top in (d)).

a focused-ion-beam (FIB) technique that makes use of Ga-ions to etch Si away with a high spatial precision. The regions damaged by Ga-ions were partially seen, and the core part of the particles was demolished. However, chemical etching was mostly carried out to the position where the center of Si particles is located. (Fig. 2(b) and (c)). Immediately after chemical etching, a very thin layer of silicon oxide formed on the Si surface, as indicated in the X-ray diffraction (XRD) pattern (bottom of Fig. 2(d)). When as-synthesized mSi was immersed in 5% HF solution for 1 min, the silicon oxide was completely removed (top of Fig. 2(d)).

3.2 Carbon-coating and characterization of multi-dimensional bulk Si anodes

Bulk Si anodes have not sustained a large volume expansion of >300%, and their pulverization results in the loss of interparticle electronic contact and capacity fade. Carbon coating has been used as a useful tool because of its excellent electrochemical conductivity, relatively low mass and small volume expansion.[6] Various methods, such as chemical or physical vapor deposition,[12] mechanical milling,[31] and pyrolytic process from carbon source materials,[32,33] have been employed for preparing Si/carbon (Si/C) composite anodes. Recently, Magasinski *et al.* designed Si deposited, rigid carbon spheres with open interconnected internal channels *via* a chemical vapor deposition (CVD) synthetic route, in which the particle size, pore size, and composition of the Si/C were tuned by controlling the Si and carbon CVD process parameters. The advantages of carbon (long cycling) and Si (high capacity) were combined to improve the electrochemical performance of the anodes.[12]

We used a thermal decomposition process of acetylene gas, which is one the most popular processes, performed at 900 °C for 30 min in a quartz furnace to coat the carbon layer on the surface of etched Si powder.[6] Carbon contents of 28 wt% were measured by elemental analysis. Without perturbing the Si structures, the carbon layer was coated inside the Si pores and onto the Si surface (Fig. 3(a) and (b)). Before carbon coating, the Brunauer–Emmett–Teller (BET) specific surface area of mSi powder that is confirmed by the N_2 adsorption/desorption isotherm is 13.1 $m^2 g^{-1}$. Compared with Si nanoparticles that have BET surface areas of >30 $m^2 g^{-1}$, its value is small. This low surface area is due to that the multi-dimensional Si powder mainly consists of nanopores instead of mesopores. It should be noted that nanoparticles have difficulties for use in real Li-ion batteries because of low electrode density, and difficulty of processing, and side reactions with the electrolytes at elevated temperatures.

After carbon coating, the surface area was significantly decreased to 4.5 $m^2 g^{-1}$, indicating that most nanopores were filled with carbon layers. A TEM image of isolated Si nanowires (upper inset of Fig. 3(a)) and a magnified SEM image (lower inset of Fig. 3(a)) showed carbon layers uniformly coated on the surface of Si nanowires. A cross-section of carbon-coated mSi (c-mSi) powder obtained from the FIB process showed the spatial locations of the carbon layer and Si due to a big difference in electron densities of each component. Bright and dark regions correspond to Si and carbon, respectively (Fig. 3(b)).

The energy-dispersive X-ray spectroscopy (EDAX) pattern of c-mSi powder shows a negligible amount of oxygen that may be

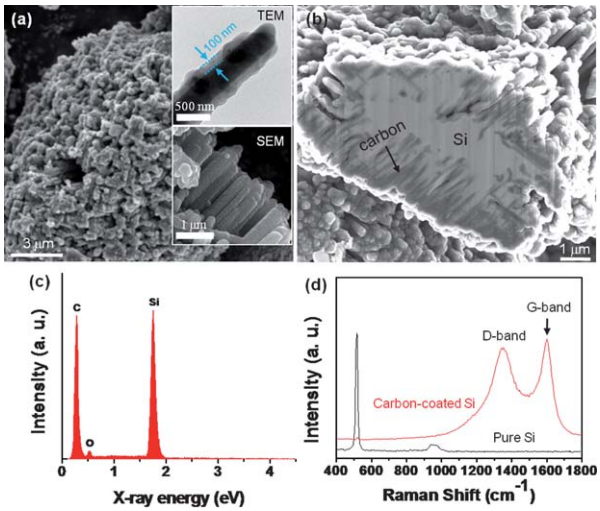

Fig. 3 The morphology and characterization of c-mSi particles. (a) A SEM image of c-mSi. Carbon layers were coated onto the Si surface and inside the pores. The inset at the top of (a) is a TEM image showing the carbon layers (carbon content of 28 wt%). The inset at the bottom of (a) is a magnified SEM image of c-mSi keeping the original morphology. (b) Cross-sectional SEM images of c-mSi obtained from the FIB process. The carbon layers are clearly seen near the Si core. (c) EDAX spectra of the c-mSi sample. A negligible amount of oxygen was detected after carbon-coating. (d) Raman spectra of the c-mSi sample. The ratio of the D band to the G band was estimated to be 2.1, indicating an amorphous carbon structure.

formed during the thermal decomposition process (Fig. 3(c)). These results indicate that the thermal decomposition process is an effective route for filling the empty space of etched Si powder with the carbon layer. Raman scattering of the c-mSi powder shows two peaks at ~1360 and ~1580 cm^{-1} corresponding to the D (disordered) band and the G (graphene) band, respectively (top spectrum of Fig. 3(d)). The ratio of the D band to the G band was estimated to be 2.1, indicating an amorphous carbon structure.[5] Here, we cannot rule out the possibility of the formation of acetylene black nanoparticles. However, we have carried out thermal decomposition of acetylene gas at a certain temperature (700–1000 °C) for only 30 min, and therefore nucleation of the acetylene black nanoparticles was minimized.

Without carbon coating, a typical Si peak appearing at 520 cm^{-1} was seen in the bottom of Fig. 3(d). Also, a peak of SiO_2 appearing at 1000–1100 cm^{-1} was not observed in the detection limit (100 ppm) of FT-IR. Moreover, we investigated the effect of carbon coating conditions on the electrochemical performance. Raman and FT-IR spectra of three different samples carbon-coated at 700, 900, and 1000 °C represent the degree of graphitization and the extent of decomposition of acetylene gas. The mSi carbon-coated at 900 °C shows a higher degree of graphitization and superior electrochemical performance compared to mSi carbon-coated at 700 and 1000 °C (ESI, Fig. S3†).

3.3 Electrochemical performance of carbon-coated multi-dimensional bulk Si anodes

Fig. 4(a) shows the voltage profiles of the c-mSi electrodes with a carbon content of 28 wt% (seen in Fig. 3(a)) at 0.1 C rate

between 1.2 V and 0.01 V in a coin-type half cell. The first discharge and charge capacities are 2440 and 2150 mAh g^{-1}, respectively, indicating a coulombic efficiency of 88%. The improved efficiency of the c-mSi compared to the nanoscale Si/C composites (71%)[34] or Si nanowires attached to current collector (79%)[2] may be associated with the carbon coating layer, which may decrease side reactions with the electrolyte.[35] This value is similar to those obtained from three-dimensional porous c-Si (88%)[13] and c-Si nanotubes (89%).[14]

The remarkable coulombic efficiency of the first cycle might be due to the uniformly coated carbon layer, which minimizes the direct contact between the Si and electrolyte, and expedites the formation of the stable solid/electrolyte interface (SEI) layer inside the pores and on the surface of c-Si particles.

After the first cycle, the coulombic efficiency maintains a high value of >98% throughout whole cycles. It seems that the film formed on the Si surface remained intact. The capacity after 20 cycles was 1850 mAh g^{-1}, corresponding to capacity retention of 86% (Fig. 4(b)). The cycling retention of bare Si, bare c-Si, mSi, and c-mSi to 20 cycles at 0.1 C rate between 1.2 and 0.01 V were compared in Fig. 4(b). The first cycle discharge capacities are 4180, 2570, 4200, and 2440 mAh g^{-1} for the electrodes of bare Si, bare c-Si, mSi, and c-mSi, respectively, with the corresponding first charge capacities of 2060, 1910, and 1490, and 2150 mAh g^{-1}. Therefore, the corresponding coulombic efficiencies in the first cycle are 49, 74, 34, and 88% for the four different Si samples, respectively. In the cases of bulk Si and c-Si, rapid capacity fade is observed, resulting in a reversible capacity lower than 1000 mAh g^{-1} in the 5th cycle by pulverization due to a large volume expansion/contraction during lithiation/delithiation process, as expected.[6] Since mSi without carbon coating has a high surface area of 13.1 m^2 g^{-1}, it may lead to more significant side reactions with the electrolyte, and more difficulty maintaining electronic contact between the Si particles, resulting in the poor coulombic efficiency and cycling performance. In contrast, the introduction of a carbon layer on the mSi alleviated the large volume expansion and thus obtained better capacity retention. When carbon-coated Si particles contain porous structures, like 3D porous structures,[13] nanotubes,[14] and hollow spheres,[15] these pores act as a buffer layer for the large volume expansion during cycling, thus they show excellent capacity retention. In the similar manner, the nanopores in c-mSi particles and the carbon layer on the surface of Si alleviated the volume changes during lithiation and delithiation, and led to superior cycling performance with high lithium storage capacity.

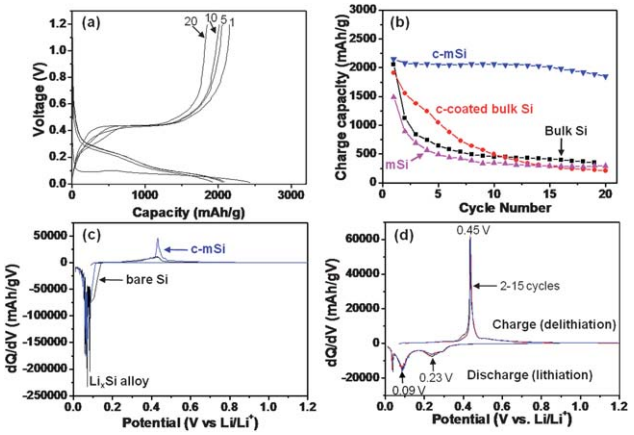

Fig. 4 Electrochemical properties of c-mSi electrodes. (a) Voltage profiles for the 1st, 2nd, 10th, and 20th cycles of the etched Si at a 0.1 C rate. (b) The cycle retention of bulk Si (square), c-coated (28 wt%) bulk Si (circle), mSi (triangle), and c-mSi (inverted triangle) are seen. (c) Differential capacity curves of bare Si and c-mSi in the first cycle. (d) Differential capacity curves of c-mSi after the first cycle. Upon lithiation process, amorphous phase transition between amorphous Li_xSi phases was observed at 0.23 and 0.09 V, while the peak corresponding to the phase transition of amorphous Li_xSi from the crystalline $Li_{15}Si_4$ phase was seen at 0.04 V in the delithiation.

Fig. 4(c) shows differential capacity curves of bare Si and c-mSi electrodes during the first cycle, and exhibited similar peak features for the two electrodes below 0.3 V *versus* Li/Li^+, which is due to the formation of lithiated amorphous Si.[36] However, the first cathodic peak was shifted from 0.12 V (bare Si) to 0.09 V (c-mSi) due to the formation of SEI layers, and it is anticipated that this will have an effect on the surface kinetics.[37] Upon the second lithiation process, three peaks were observed at 0.23, 0.09, and 0.04 V. The broad peaks at 0.23 and 0.09 V are attributed to the phase transition between amorphous Li_xSi phases, while the peak appearing at 0.04 V is assigned to the phase transition of amorphous Li_xSi from the crystalline $Li_{15}Si_4$ phase.[36] Conversely, during the charging process, a narrower peak at 0.45 V that corresponds to the formation of delithiated amorphous Si is seen (Fig. 4(d)). A delithiation peak at 0.3 V observed in micro-scale Si,[7] mesoporous Si,[38] and Si nanowires[2] was not seen. It should be noted that the c-mSi electrode maintained high reversibility after the first cycle and improved Li extraction kinetics, as evidenced by the increase in a peak voltage of 0.45 V compared to the first cycle.[39]

Fig. 5(a) shows the SEM image of c-mSi particles after 20 cycles. The surface of the cycled electrode exhibits a similar morphology to that of the pristine sample, except for the formation of SEI layers, as seen in the magnified SEM image (Fig. 5(b)). The TEM image of each nanowire shows that mesopores in the nanowires were merged to make a nanotube-shaped morphology (Fig. 5(c)). The HR-TEM image captured from the several different regions indicates that crystalline Si was completely transformed to amorphous Si (Fig. 5(d)). It has been reported that the initial crystalline Si phase is transformed into amorphous Si after the initial cycles.[36,40] Nonetheless, the diameter of Si nanowires after cycling is nearly the same as the pristine Si nanowires, since the nanopores act as a buffer layer for the volume changes. The selected-area diffraction pattern also confirmed the amorphous Si structures, as the evidence of an isotropic ring pattern (Fig. 5(e)). The XRD pattern is further evidence of the formation of amorphous Si over wide areas. After cycling, crystalline Si peaks completely disappeared, and only copper peaks used as a current collector were seen (Fig. 5(f)).

Since the heavily carbon-coated (28 wt%) mSi anodes do not exhibit sufficient discharge capacities in the first cycle as seen in Fig. 4(b), the effect of thickness of the carbon-coating layer on the discharge/charge capacity of mSi anodes was investigated. Fig. 6(a) shows SEM images of mSi with a carbon content of ~15 wt%. Because a thin carbon layer was coated on the surface of the mSi, the morphology of the original etched Si can clearly be seen in the inset of Fig. 6(a). To investigate morphologies of porous

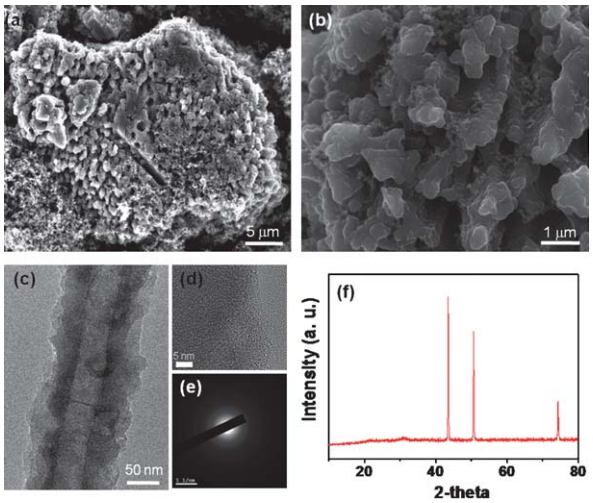

Fig. 5 The morphology of c-mSi electrodes after cycling. (a) A SEM image of c-mSi electrodes after 20 cycles. (b) A magnified image of the sample seen in the Fig. 5(a). The pulverization of the Si nanowires is not observed, but SEI layers coated on the Si surface were seen. (c) A TEM image of c-mSi obtained by ultrasonication after removing SEI layers in H_2SO_4. (d) A magnified TEM image and (e) the selected area diffraction pattern showing amorphous Si, after cycling. (f) An XRD pattern of cycled Si. Only copper peaks used as current collector were seen with disappearance of Si peaks due to the formation of amorphous Si.

c-Si nanowires, the samples were dispersed in ethanol by ultrasonication. The TEM image shows that a thin carbon layer with thickness of 10–20 nm was uniformly coated on the porous Si nanowires (Fig. 6(b)). Subsequently, the electrochemical performance of the c-mSi was investigated. Fig. 6(c) shows the voltage profiles of the c-mSi electrodes at various C rates from 0.1 C to 3 C rate (discharge rate was fixed at 0.1 C) between 1.2 V

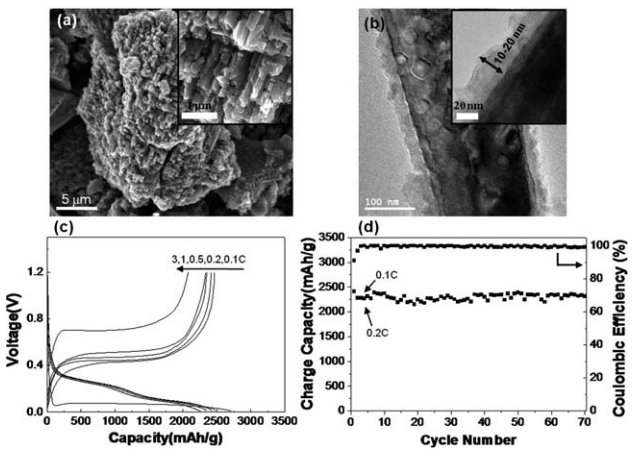

Fig. 6 The morphology of mSi electrodes with a thin carbon layer and the cycling performance. (a) A SEM image showing mSi with a carbon content of ~15 wt%. The inset in of (a) is a magnified SEM image showing the morphology of mSi similar to that of original etched Si. (b) A TEM image of c-mSi. The inset in (b) is a magnified TEM image showing the 10–20 nm thick carbon layer on the surface of the Si wires. (c) Voltage profiles of c-mSi having a thin carbon layer at various C rates from 0.1 to 3 (discharge rate was fixed at 0.1 C). (d) Charge capacity *versus* cycle number for the c-mSi at a rate of 0.2 C after the first cycle at 0.1 C rate.

Table 1 Volumetric energy densities of c-mSi and c-Si electrodes

Sample[a]	Thickness of electrode before lithiation	Thickness of electrode after lithiation	Mass of active materials	Volumetric energy density
c-mSi	~20 μm	~30 μm	~9 mg	~3600 mAh cc^{-1}
c-Si	~20 μm	~45 μm	~9 mg	~2400 mAh cc^{-1}

[a] Area of electrode: 2 cm^2.

and 0.01 V in a coin-type half cell. The first discharge and charge capacities are 2660 and 2410 mAh g^{-1} at a rate of 0.1 C, respectively, indicating a high coulombic efficiency of 91%. Even at a high rate of 3 C, a capacity retention of 84% was seen compared to that of the 0.1 C rate. Moreover, the capacity retention of c-mSi electrodes after 70 cycles was 95% at a rate of 0.2 C after pre-cycling at 0.1 C (Fig. 6(d)). When an appropriate thick carbon layer was coated onto the mSi electrodes, the superior electrochemical performance including a high specific capacity, a stable cycling retention, and excellent rate capability was significantly improved. Also, it results in a significantly enhanced the volumetric energy density in the c-mSi electrodes (~3600 mAh cc^{-1}) compared to c-Si (~2400 mAh cc^{-1}), as summarized in Table 1.

4. Conclusions

We produced multi-dimensional Si electrodes composed of porous nanowires and micro-sized cores with nano-sized pores from commercially available bulk Si powder using a metal-assisted chemical etching process. The synthetic route is a simple, scalable (high yield of 40–50%), and cost effective way to make high-performance Si anode materials in lithium-ion batteries. Carbon-coated multi-dimensional Si electrodes accommodate large volume expansion/contraction during lithiation/delithiation process. These materials showed a high reversible charge capacity of ~2400 mAh g^{-1} with coulombic efficiency of 91% and stable cycling performance. This approach opens up an effective method for fabrication of high-performance anode materials in lithium-ion batteries.

Acknowledgements

This work was supported by the Converging Research Center Program through the Ministry of Education, Science and Technology (2010K000984) and the WCU (R31-2008-000-20012-0).

Notes and references

1 G.-A. Nazri and G. Pistoia, *Lithium Batteries: Science and Technology*. Kluwer Academic/Plenum, Boston, 2004.
2 C. K. Chan, H. Peng, G. Liu, K. McIlwrath, X. F. Zhang, R. A. Huggins and Y. Cui, *Nat. Nanotechnol.*, 2008, **3**, 31.
3 M.-S. Park, G.-X. Wang, Y.-M. Kang, D. Wexler, S.-X. Dou and H.-K. Liu, *Angew. Chem., Int. Ed.*, 2007, **46**, 750.
4 M.-H. Seo, M. Park, K. T. Lee, K. Kim, J. Kim and J. Cho, *Energy Environ. Sci.*, 2011, **4**, 425.
5 H. Lee and J. Cho, *Nano Lett.*, 2007, **7**, 2638.
6 U. Kasavajjula, C. Wang and A. J. Appleby, *J. Power Sources*, 2007, **163**, 1003.
7 M. N. Obrovac and L. J. Krause, *J. Electrochem. Soc.*, 2007, **154**, A103.

8 C. Liu, F. Li, L.-P. Ma and H.-M. Cheng, *Adv. Mater.*, 2010, **22**, E28.
9 P. G. Bruce, B. Scrosati and J.-M. Tarascon, *Angew. Chem., Int. Ed.*, 2008, **47**, 2930.
10 M. G. Kim and J. Cho, *Adv. Funct. Mater.*, 2009, **19**, 1497.
11 A. S. Aricò, P. Bruce, B. Scrosati, J.-M. Tarascon and W. van Schalkwijk, *Nat. Mater.*, 2005, **4**, 366.
12 A. Magasinski, P. Dixon, B. Hertzberg, A. Kvit, J. Ayala and G. Yushin, *Nat. Mater.*, 2010, **9**, 353.
13 H. Kim, B. Han, J. Choo and J. Cho, *Angew. Chem., Int. Ed.*, 2008, **47**, 10151.
14 M.-H. Park, M. G. Kim, J. Joo, K. Kim, J. Kim, S. Ahn, Y. Cui and J. Cho, *Nano Lett.*, 2009, **9**, 3844.
15 H. Ma, F. Cheng, J.-Y. Chen, J.-Z. Zhao, C.-S. Li, Z.-L. Tao and J. Liang, *Adv. Mater.*, 2007, **19**, 4067.
16 J. C. Park, J. Kim, H. Kwon and H. Song, *Adv. Mater.*, 2009, **21**, 803.
17 H.-L. Zhang, *Carbon*, 2006, **44**, 2778.
18 Y. Yu, C.-H. Chen and Y. Shi, *Adv. Mater.*, 2007, **19**, 993.
19 Y. Sugiyama, H. Okamoto, T. Mitsuoka, T. Morikawa, K. Nakanishi, T. Ohta and H. Nakano, *J. Am. Chem. Soc.*, 2010, **132**, 5946.
20 C. K. Chan, R. N. Patel, M. J. ÓConnell, B. A. Korgel and Y. Cui, *ACS Nano*, 2010, **4**, 1443.
21 Z. Bao, M. R. Weatherspoon, S. Shian, Y. Cai, P. D. Graham, S. M. Allan, G. Ahmad, M. B. Dickerson, B. C. Church, Z. Kang, H. W. Abernathy III, C. J. Summers, M. Liu and K. H. Sandhage, *Nature*, 2007, **446**, 172.
22 S. K. Bux, M. Rodriguez, M. T. Yeung, C. Yang, A. Makhluf, R. G. Blair, J.-P. Fleuial and R. B. Kaner, *Chem. Mater.*, 2010, **22**, 2534.
23 B. Bang, H. Kim, J.-P. Lee, J. Cho and S. Park, *Energy Environ. Sci.*, 2011, **4**, 3395.
24 X. Zhong, Y. Qu, Y.-C. Lin, L. Liao and X. Daun, *ACS Appl. Mater. Interfaces*, 2011, **3**, 261.
25 K. Peng, J. Jie, W. Zhang and S.-T. Lee, *Appl. Phys. Lett.*, 2008, **93**, 033105.
26 W. Xu and J. C. Flake, *J. Electrochem. Soc.*, 2010, **157**, A41.
27 S. Koynov, R. N. Pereira, I. Crnolatac, D. Kovalev, A. Huygens, V. Chirvony, M. Stutzmann and P. de Witte, *Adv. Eng. Mater.*, 2011, **13**, B225.
28 A. Loni, D. Barwick, L. Batchelor, J. Tunbridge, Y. Han, Z. Y. Li and L. T. Canham, *Electrochem. Solid-State Lett.*, 2011, **14**, K25.
29 T. Qiu and P. K. Chu, *Mater. Sci. Eng., R*, 2008, **61**, 59.
30 Y. Qu, L. Liao, Y. Li, H. Zhang, Y. Huang and X. Duan, *Nano Lett.*, 2009, **9**, 4539.
31 C. S. Wang, G. T. Wu, X. B. Zhang, Z. F. Qi and W. Z. Li, *J. Electrochem. Soc.*, 1998, **145**, 2751.
32 A. M. Wilson, J. N. Reimers, E. W. Fuller and J. R. Dahn, *Solid State Ionics*, 1994, **74**, 249.
33 D. Larcher, C. Mudalige, A. E. George, V. Porter, M. Gharghouri and J. R. Dahn, *Solid State Ionics*, 1999, **122**, 71.
34 S.-H. Ng, J. Wang, D. Wexler, K. Konstantinov, Z.-P. Guo and H.-K. Liu, *Angew. Chem., Int. Ed.*, 2006, **45**, 6896.
35 Y.-S. Hu, R. Demir-Cakan, M.-M. Titirici, J.-O. Müller, R. Schlögl, M. Antonietti and J. Maier, *Angew. Chem., Int. Ed.*, 2008, **47**, 1645.
36 J. Li and J. R. Dahn, *J. Electrochem. Soc.*, 2007, **154**, A156.
37 W.-R. Liu, J.-H. Wang, H.-C. Wu, D.-T. Shieh, M.-H. Yang and N.-L. Wu, *J. Electrochem. Soc.*, 2005, **152**, A1719.
38 H. Kim and J. Cho, *Nano Lett.*, 2008, **8**, 3688.
39 S. H. Ng, J. Wang, D. Wexler, S. Y. Chew and H. K. Liu, *J. Phys. Chem. C*, 2007, **111**, 11131.
40 Y.-M. Kang, J.-Y. Go, S.-M. Lee and W.-U. Choi, *Electrochem. Commun.*, 2007, **9**, 1276.